Numerical study on Rayleigh-Taylor effect on cylindrically converging Richtmyer-Meshkov instability

ZhiGang Zhai[1*], Fu Zhang[2], ZhangBo Zhou[1], JuChun Ding[1], and Chih-Yung Wen[3]

[1]*Department of Modern Mechanics, University of Science and Technology of China, Hefei 230026, China;*
[2]*Beijing Institute of Space Long March Vehicle, Beijing 100076, China;*
[3]*Department of Mechanical Engineering, The Hong Kong Polytechnic University, Hong Kong 999077, China*

Evolution of a two-dimensional air/SF_6 single-mode interface is numerically investigated by an upwind CE/SE method under a cylindrically converging circumstance. The Rayleigh-Taylor effect caused by the flow deceleration on the phase inversion (RTPI) is highlighted. The RTPI was firstly observed in our previous experiment, but the related mechanism remains unclear. By isolating the three-dimensional effect, it is found here that the initial amplitude (a_0), the azimuthal mode number (k_0) and the re-shocking moment are the three major parameters which determine the RTPI occurrence. In the variable space of (k_0, a_0), a critical a_0 for the RTPI occurrence is solved for each k_0, and there exists a threshold value of k_0 below which the RTPI will not occur no matter what a_0 is. There exists a special k_0 corresponding to the largest critical a_0, and the reduction rule of critical a_0 with k_0 can be well described by an exponential decay function. The results show that the occurrence of the RTPI requires a small a_0 which should be less than a critical value, a large k_0 which should exceed a threshold, and a right impinging moment of the re-shock which should be later than the RTPI occurrence. Finally, the effects of the incident shock strength, the density ratio and the initial position of the interface on the threshold value of k_0 and on the maximum critical a_0 are examined. These new findings would facilitate the understanding of the converging Richtmyer-Meshkov instability and would be helpful for designing an optimal structure of the inertia confinement fusion capsule.

converging shock wave, Rayleigh-Taylor effect, Richtmyer-Meshkov instability

1 Introduction

Richtmyer-Meshkov (RM) instability occurs when an initially perturbed interface separating two different fluids is accelerated by a shock wave [1, 2], and plays a central role in understanding the hydrodynamic processes involved in inertial confinement fusion (ICF) [3], supersonic combustion [4] and supernova explosions [5]. The RM instability primarily results from the baroclinic vorticity caused by the misalignment of the pressure gradient across the shock with the density gradient across the interface. The induction of the baroclinic forces also dominates the Rayleigh-Taylor (RT) instability [6] in which the pressure gradient is caused by a force field. Unlike the RT instability where the perturbation can be either unstable or stable depending on whether the acceleration is directed from the lighter fluid to the heavier one or vice versa, the perturbation in RM instability is always unstable, regardless of the direction of the shock impact.

*Corresponding author (email: sanjing@ustc.edu.cn)

During past few decades, the interaction of a planar shock with a two-dimensional (2D) single-mode interface was studied extensively [7-10]. However, the physical background of ICF cares more about the interaction of a converging shock with a disturbed interface. As a result, the converging RM instability has become an imperative [11, 12]. Compared with the planar RM instability in which only the spanwise direction is involved, the converging RM instability is much more complicated because both the radial and angular directions need to be considered. Based on the linear model of small disturbance proposed by Taylor [6] for the planar RT stability, Bell [13] and Plesset [14] respectively extended the linear model to cylindrical and spherical cases following the incompressible hypothesis. In the cylindrical geometry, the development of a single-mode disturbance is described by

$$a_{tt} + 2\frac{R_t}{R}a_t + (k_0A + 1)\frac{R_{tt}}{R}a = 0, \tag{1}$$

where a is the perturbation amplitude, k_0 is the azimuthal mode number, A is Atwood number defined as $A = (\rho_2 - \rho_1)/(\rho_2 + \rho_1)$ with ρ_1 and ρ_2 being the densities of the incident and transmitted fluids, respectively, R is mean cylindrical radius of the moving interface and is usually defined as the radius of an unperturbed interface. The subscript 't' represents the derivative of quantity with respect to time, and similarly hereinafter. In this formula, the interface radius R varies with time, which is the major difference from the planar RT instability. This geometrical effect is called Bell-Plesset (BP) effect and it disappears when R tends to infinity. To deal with the compressible case, Bell suggested that a uniform compression term ρ_t/ρ, which satisfies the potential equation $\nabla^2\Phi = -\rho_t/\rho$ with Φ the potential function and ρ the average value of ρ_1 and ρ_2, stands for the compressibility. Thus, the formula is re-derived here as:

$$a_{tt} + \left(2\frac{R_t}{R} + \frac{\rho_t}{\rho}\right)a_t + \left[(k_0A + 1)\frac{R_{tt}}{R} + \frac{\rho_t R_t}{\rho R} + \frac{\rho\rho_{tt} - {\rho_t}^2}{\rho^2}\right]a = 0. \tag{2}$$

In the converging RM instability, the impact of imploding shock will result in an instantaneous increment for the convection velocity of interface $R_t(0^+)$ and the growth rate of perturbation $a_t(0^+)$. Following the impulsive model by Richtmyer [1], Mikaelian [15] put forward an incompressible equation by regarding the shock as an impulsive acceleration ($g = R_{tt} = \Delta v\delta t$) with Δv the interface velocity jump induced by the shock and neglecting the weak change of the convection velocity in the early stage,

$$a(t) = (0^+)\left[1 + (k_0A^+ + 1)\left(\frac{R_0}{R} - 1\right)\right],$$
$$a_t = a(0^+)(k_0A^+ + 1)\Delta v\frac{R_0}{R^2}, \tag{3}$$

with R_0 the initial interface radius and A^+ the post-shock Atwood number. Recently, some simplifications have been implemented to analyze the coupled features between nonlinear effect and BP effect in the nonlinear stage [16-19]. A common feature of these models is that the BP effect offsets a part of the feedback from high-order nonlinearity to the fundamental mode, which extends the linear stage compared with the planar RM instability, coinciding with the result of laser driven experiment [20]. Some numerical work [21-23] focused on the effect of the reflected shock which is inevitable in the converging RM instability. Actually, before the reshock (the interaction of the reflected shock from center with the interface), the convection velocity of the shocked interface is unsteady. Therefore, the third term R_{tt} in eq. (1) will continuously contribute to the interface development compared with the planar RM instability. This additional effect in converging geometry will cause RT instability or stability depended on whether the lighter fluid accelerates heavier fluid or vice versa. Therefore, the coupling of BP effect, RT effect, RM instability and reshock greatly complicates the converging RM instability.

At early stages of the converging RM instability, the convection velocity of interface varies little, and eq. (3) provides a fairly good description of the perturbation evolution. When the interface approaches the focusing point, the pressure gradient in the radial direction is so notable that the RT effect cannot be ignored any more. Lombardini et al. [24, 25] performed large-eddy simulations of turbulent mixing about spherically converging RM instability, and indicated that the RT instability appears during the circulatory velocity-variation process and the baroclinic instabilities (RM and RT) dominate the perturbation growth on the whole evolutionary process when the convergence ratio is far less than 30. In our previous work [26], the interaction of a cylindrically converging shock with an air/SF_6 interface was experimentally studied, and the interface amplitude was found to decrease continuously and even to be negative before the reshock, which was ascribed to the strong and long-term effect of RT stabilization (RT-induced phase inversion, RTPI). Here we should point out that for a single shock impact, the "normal phase inversion" generally occurs for a heavy/light interface, and the "RTPI" generally occurs for a light/heavy interface with small initial amplitude and high wave number. The RTPI will be helpful to find a freezing interface in ICF, and needs further investigations. Unfortunately, the soap film technique created a three-dimensional (3D) interface in our experiment, and it was difficult to discriminate the RT stabilization effect from the 3D effect on the RTPI since both of them contribute to the decline of the amplitude growth. Meanwhile, it was concluded that this RTPI occurs only when the initial perturbation amplitude is small enough. However,

the mechanism and the dominant parameters of the RTPI such as how small the initial perturbation can trigger the RTPI remain unclear. In this work, we aim to numerically investigate the evolution of a 2D single-mode interface in a cylindrical geometry to eliminate the 3D effect such that the RT stabilization effect on the RTPI is emphasized. The first step is to find whether a critical state exists for the RTPI emergence in a large range of initial wavenumber and initial amplitude, and then the influences of other initial parameters such as the incident shock strength, Atwood number and initial location of the interface on the RTPI will be examined.

2 Numerical method

To describe the compressible multi-component flow problem, we employ a quasi-conservative five-equation model [27]. The governing equations of the volume fraction-based five-equation model [28] can then be expressed as:

$$\begin{aligned}
&\frac{\partial \alpha_i}{\partial t} + \boldsymbol{V}\cdot\nabla\alpha_i = 0,\ i = 1 \text{ or } 2,\\
&\frac{\partial \rho_i\alpha_i}{\partial t} + \nabla\cdot(\rho_i\alpha_i\boldsymbol{V}) = 0,\ i = 1 \text{ and } 2,\\
&\frac{\partial \rho\boldsymbol{V}}{\partial t} + \nabla\cdot(\rho\boldsymbol{V}\otimes\boldsymbol{V} + p\boldsymbol{I}) = 0,\ \otimes \text{ is the Kronecker product},\\
&\frac{\partial E}{\partial t} + \nabla\cdot[\boldsymbol{V}(E+p)] = 0,
\end{aligned} \tag{4}$$

where α_i denotes the volume fraction of fluid i, ρ_i the density of fluid i, ρ the density of the mixture, $\boldsymbol{V}$ the velocity vector, p the pressure, E the total energy and $\boldsymbol{I}$ the unit matrix. The equation of state of perfect gas is employed to close the system,

$$p = (\gamma - 1)(E - \frac{1}{2}\rho\boldsymbol{V}\cdot\boldsymbol{V}), \tag{5}$$

where

$$\frac{1}{\gamma - 1} = \Sigma\frac{\alpha_i}{\gamma_i - 1}. \tag{6}$$

The total density and the sound speed of the mixture can be respectively calculated as:

$$\rho = \Sigma\alpha_i\rho_i,\ c = \sqrt{\gamma(p)/\rho}. \tag{7}$$

We note that this model can prevent pressure oscillation across an interface separating two materials.

The five-equation model is solved by an upwind space-time conservation element and solution element (CE/SE) scheme with second-order accuracy in both temporal and spatial scales [29, 30]. The upwind CE/SE scheme is a minor modification of the centered CE/SE scheme originally proposed by Chang [31] such that it inherits most properties of the central scheme and significantly improves the calculation accuracy of the contact discontinuities by introducing an upwind flux in the evaluation of spatial derivatives. The rotated HLLC flux which can sharply capture the interfaces and achieve carbuncle-free results is adopted in this study. Furthermore, a simple limiter is employed to strictly preserve the positivity of volume fractions without loss of accuracy and conservativeness [32]. The detailed descriptions and extensive verifications and applications on complex flow can be found in the references [29, 30, 32-34].

We first perform a validation of the numerical method by comparing numerical results with our previous experiments [35], in which a cylindrically converging shock interacting with unperturbed and perturbed cylindrical interfaces was investigated. These experiments present nice 2D feature. In numerical configuration, a 90° computational domain with the dimensions of 50 mm × 50 mm, as sketched in Figure 1, is adopted. As a result, if an initial perturbed interface is involved, the interface must be perpendicular to the upper and right walls (crest or trough) to avoid the reflection from the walls, i.e., the azimuthal mode number adopted in the computational domain should be an even number. The initial discontinuous interface sharply separates SF_6 inside from air outside, and both gases are assumed to be perfect gases at initial temperature and pressure of 298 K and 101325 Pa, respectively. A uniform state behind the initially imploding shock is considered, in which the density, pressure and radial velocity are calculated from Rankine-Hugoniot relation. The reflection conditions are applied to right and top boundaries, while non-reflection conditions to left and bottom boundaries. To avoid the possible singularity of two different boundary conditions on the left-top and right-bottom corners, the virtual mesh points on top and right boundaries close to the corners are specified as inflow condition. In this way, the meshes at the corners are dealt with the same boundary condition in both x and y directions, which eliminates the singularity. Note

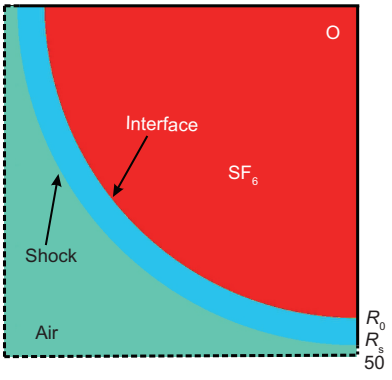

Figure 1 (Color online) The schematic of the computational domain and boundary condition of unperturbed case. The solid and dashed lines represent the reflective and non-reflective boundaries, respectively.

that this treatment produces a negligible influence on the whole instability development.

In experiments, the gas inside is not pure SF_6 but a mixture of SF_6 and air. Based on the velocities of the incident shock wave and the transmitted shock waves, the properties of the mixture inside the interface will be firstly determined according to one-dimensional gas dynamics theory. The comparison of the experiments with the numerical simulations will provide more accurate values of the properties. The properties of the mixture and the numerical parameters are listed in Table 1, which are the same as those in experiments [35]. Before computations, the grid convergence is checked. The density profiles for different rectangular mesh sizes along the radius direction at $t = 50$ μs after a converging shock impinging an unperturbed cylindrical air/SF_6 interface are considered. The initial conditions are the same as those in unperturbed case in our previous experiments. As presented in Figure 2, the density profiles are convergent as the mesh size reduces. To save the computational cost, the mesh size of 0.1 mm is chosen. However, for the cases with high wave numbers, the mesh size is refined to 0.05 or 0.025 mm. Qualitative and quantitative comparisons of movements of shock waves and interface during the interaction of a converging shock with an unperturbed interface are given in Figures 3 and 4. Generally a good agreement is achieved. Further, the shock behaviors and interface morphologies after a converging shock interacting with a perturbed interface with three different initial amplitudes (a_0 = 1, 2 and 3 mm) are compared. Take the experiment (a_0 = 1 mm) as an example for comparing the interface morphology and wave pattern. As shown in Figure 5, the numerical method nicely captures the evolution of the interface and waves. The interface amplitudes for three cases from numerical simulations are shown in Figure 6, which presents a very good agreement with the experimental measurements at all stages, including the reshock stage.

3 Results and discussion

Previous work [26, 35] showed that after the passage of a cylindrically converging shock, the movement of an unperturbed interface will experience three stages: a nearly steady phase with a constant velocity at first, an inward-moving decelerating phase before reshock, and an outward-moving decelerating phase after reshock. If the initial interface is disturbed, the RT stabilization effect (heavier fluid accelerates lighter one) during the inward-moving deceleration phase before reshock will suppress the perturbation growth, possibly causing the occurrence of phase inversion, and RT instability (lighter fluid accelerates heavier one) coupled with RM instability will dominate the flow after reshock. The physical parameters which may influence the existence of phase inversion before the reshock include the initial amplitude a_0, azimuthal mode number k_0, initial Atwood number A, shock Mach number M_0 when incident shock impacts interface, and initial interface radius R_0. In this work, the influence of a_0 on the RTPI is first under consideration while keeping other parameters fixed. Subsequently, how other parameters affect the RTPI will be discussed. In numerical setup, a 90° computational domain with the dimensions of 220 mm × 220 mm is adopted. The initial stationary cylindrical interface and imploding shock are positioned at R_0 = 195 mm and R_s = 212 mm, respectively, which are the same as those in our experiment [26]. Besides, both gases are regarded as pure in computation, differing from the experimental settings where the gas contamination must be considered. Also, nitrogen is chosen as an ambient gas in computation instead of air in experiment. The initially converging shock with an intensity of Ma = 1.25 moves inward and when it meets the interface, the intensity increases to 1.26 calculated by the CCW relation [36-38]. The other numerical settings are the same as those described in sect. 2.

3.1 Evolution of perturbed interface with different initial amplitudes

For a single-mode interface, the equation of interface shape can be described as $r = R_0 + a_0 \cos(k_0\theta)$. Here we will first discuss the influence of a_0 on the RTPI by keeping other parameters (M_0, A, R_0, k_0) = (1.26, 0.68, 195 mm, 20) unchanged. The development of three disturbed interfaces (Cases I1, I2 and I3 with a_0 = 1.0, 1.65 and 2.0 mm, respectively) is representatively shown in Figure 7 for the detail of the interface morphology. Time-variation of interface ampli-

Table 1 Physical parameters of mixture inside for unperturbed interface and perturbed interface at temperature T_0 =298 K and pressure p_0=101325 Pa. The ambient air is considered as pure. a_0, initial amplitude; Ma, initial shock Mach number; γ, specific heat ratio; ρ, density of gas; R_s, initial position of shock from the origin; R_0, initial position of interface from the origin

Case	a_0 (mm)	Ma	γ	ρ (kg/m^3)	R_s (mm)	R_0 (mm)
Unperturbed	0	1.27	1.152	3.611	38.6	25
Perturbed-Case1	1	1.23	1.157	3.49	41.9	24.2
Perturbed-Case2	2	1.26	1.135	4.09	41.1	24.3
Perturbed-Case3	3	1.27	1.164	3.32	42.5	24.6

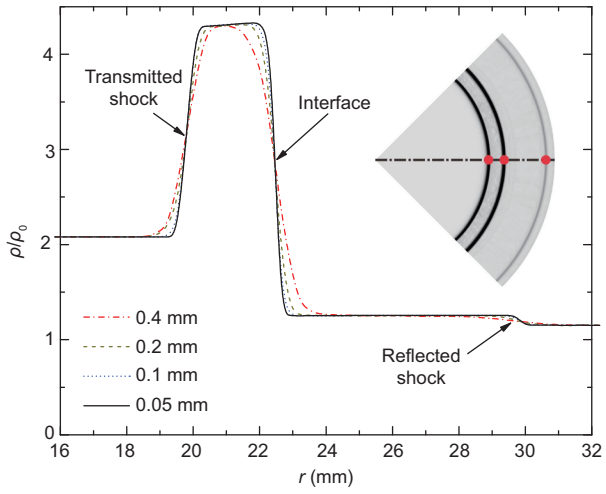

Figure 2 (Color online) The density profiles for different mesh sizes along the radius direction at $t = 50$ μs after a cylindrically converging shock wave impacting a cylindrical air/SF_6 interface.

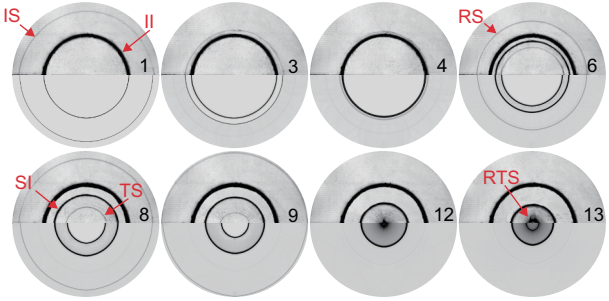

Figure 3 (Color online) Evolution of an unperturbed cylindrical air/SF_6 interface impacted by a cylindrically converging shock wave. IS, incident shock; II, initial interface; TS, transmitted shock; RS, reflected shock; SI, shocked interface; RTS, reflected transmitted-shock. Interval: 11.43 μs. Upper: experimental schlieren image; Lower: numerical schlieren image at the same instant.

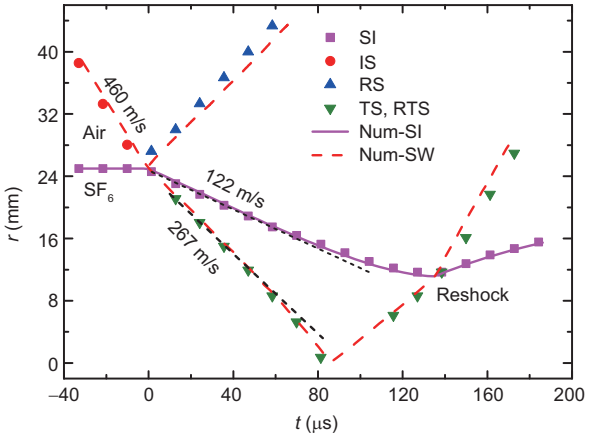

Figure 4 (Color online) Time variations of the interface displacement and shock positions. Symbols are the same as those in Figure 3. The dashed lines are used to determine the waves speeds.

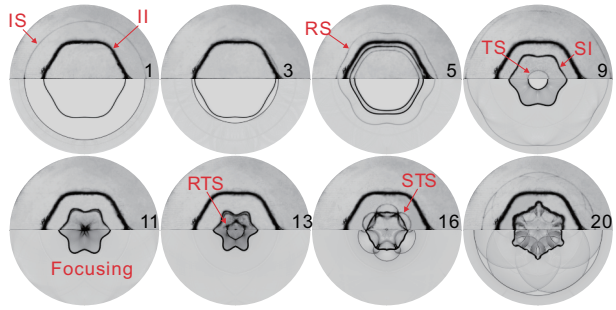

Figure 5 (Color online) The evolution of the single-mode interface for Perturbed-Case1 as listed in Table 1. Upper: experimental schlieren image; lower: numerical schlieren image at the same instant. STS, secondary transmitted shock. Other symbols have the same meaning as those in Figure 3.

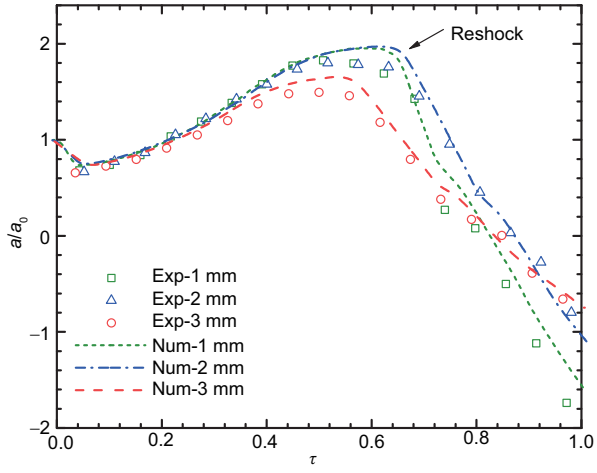

Figure 6 (Color online) Comparison of interface amplitudes between the experiments and computations for the three cases listed in Table 1.

tude, defined as $a = (r_1 - r_2)/2$ where r_1 and r_2 are respectively the varying radii of crest and trough near the diagonal as shown in Figure 7, is plotted in Figure 8(a). The amplitude evolution can also be divided into three stages after the compression, corresponding to the counterparts in undisturbed case. At the first stage, the amplitude increases because of the RM instability, and the weak convergence effect has a limited influence on the linear growth of perturbation before $t_1 \approx 820$ μs. During the second stage before reshock, the amplitude reduces for all cases owing to the RT stabilization effect which is caused by the stronger adverse pressure gradient near the geometry origin. It is observed that the amplitude in Case I1 reduces to be negative before reshock, indicating the RTPI occurrence ($t = 1356$-1434 μs). The amplitude in Case I3 is still positive before reshock, and thus the RTPI does not occur. In Case I2, the amplitude is decreased to nearly zero at reshock-time, which means that the initial amplitude in Case I2 is almost the critical value for the RTPI occurrence with other fixed initial parameters. As a result, a RTPI only occurs with small initial amplitudes, verifying our experimental

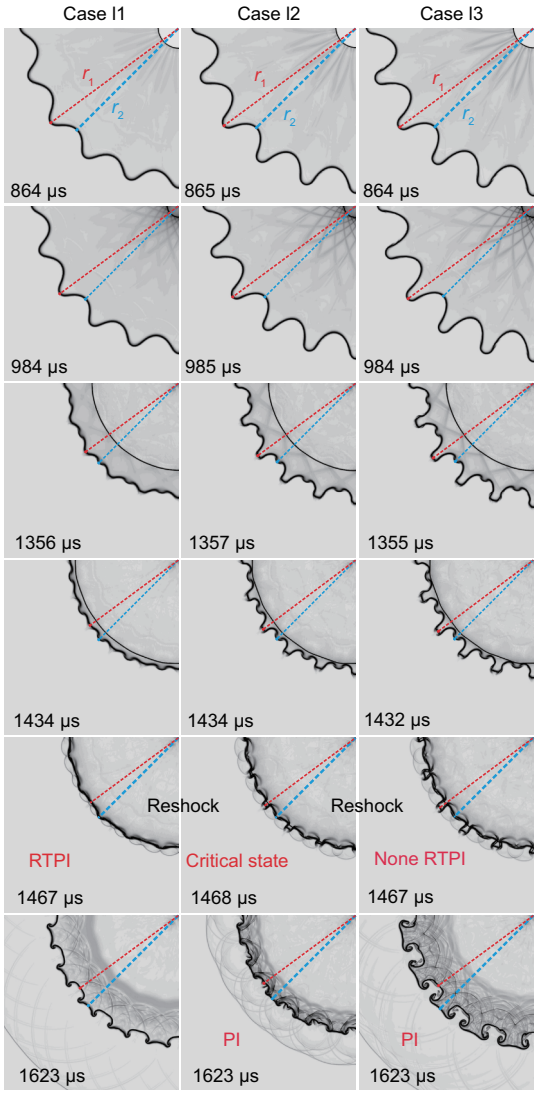

Figure 7 (Color online) The schlieren pictures showing the evolution of the single-mode interface for Cases I1, I2 and I3. PI: phase inversion.

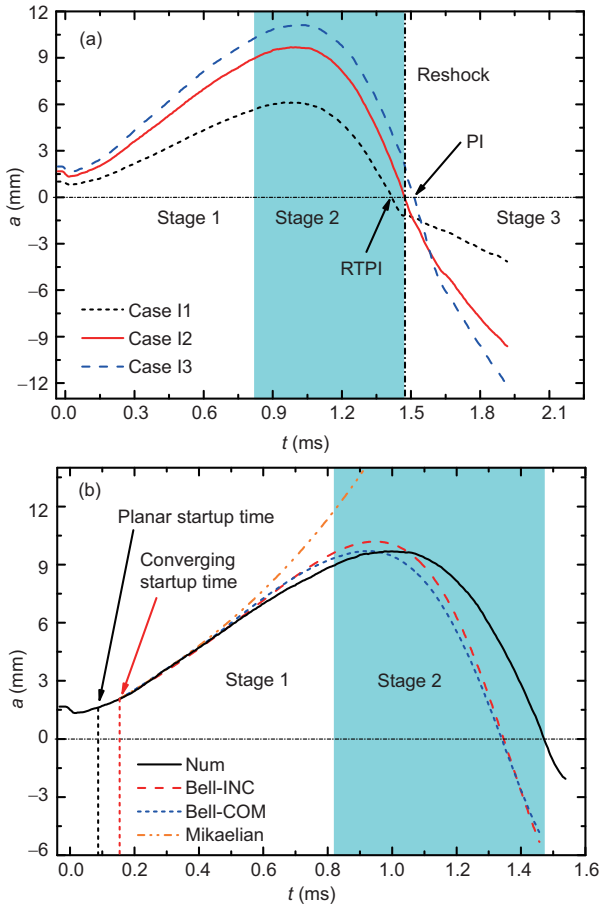

Figure 8 (Color online) Time-variation of interface amplitude in three perturbed cases (a), and comparison of amplitude growth between the numerical result and theoretical predictions from models for Case I2 (b). Bell-INC means the prediction by the incompressible Bell theory; Bell-COM means the prediction by the compressible Bell theory; Mikaelian means the prediction by the theory proposed by Mikaelian.

work. After reshock, the reflected shock facilitates the occurrence of a normal phase inversion (PI) for an SF_6/air interface in Cases I2 and I3 (t = 1467-1623 μs), while a normal PI is absent in Case I1. The RM instability caused by the reflected shock coupled with the RT instability greatly promotes the perturbation growth.

For the satisfactory of small perturbation hypothesis, three models (eqs. (1)-(3)) are applicable to predict the amplitude growth in Case I2. The numerical result shows that a startup time is needed to achieve the linear growth because the ripples from the transmitted shock and reflected shock need some times to be settled down. In a planar geometry, Lombardini and Pulllin [39] regarded the transmitted and reflected shocks as moving boundaries and considered the flow field between them as an incompressible one, putting forward a startup time as:

$$\tau = \frac{1}{2k}\left[\frac{1-A^+}{U_{s2}} + \frac{1+A^+}{-U_{s1}}\right], \tag{8}$$

where k is wave number in the planar geometry, U_{s2} and $-U_{s1}$ are speeds of reflected shock and transmitted shock relative to the interface, respectively. The prediction of startup time in the planar geometry has already been verified [39]. Similarly, we can transform the wave number in the converging geometry to that in planar geometry as $k = k_0/R_0$, and then the startup time in the converging case is estimated to be 86.5 μs. However, the numerical result reveals that a startup time of $\tau \approx 152$ μs is needed to achieve the linear growth, which is about twice over the theoretical estimation. Based on the numerical startup time in the converging case, the predictions of amplitude growth for Case I2 are shown in Figure 8(b), together with the numerical result. In the theoretical predictions, the impulsive growth rate is considered as an initial value, and the growth rates are calculated by dis-

cretely numerical integration with R, the convection velocity R_t and the acceleration R_{tt} at each discrete step. The impulsive model gives a good prediction of the linear growth rate, while the predictions from three models deviate from the numerical result before the end of stage 1. The divergence of two Bell models from the numerical result is believed to be caused by weak nonlinearity. The estimation by Mikaelian's model deviates most from the numerical result because R_t is ignored in this model. In stage 2, although both Bell models provide a correct tendency of amplitude growth, the divergence between them is amplified, which may be caused by the flow compressibility. Although a uniform compression term ρ_t/ρ around the interface is adopted to describe the compressibility in eq. (2), the real ρ_t/ρ near the geometry center or the shock is quite different from the value near the interface. It is thought that this uniform compressible assumption is inappropriate to predict the amplitude development at late stages.

In Case I1, the perturbation amplitude of the basic frequency $a(k_0)$ does not undergo a normal PI during reshock. If we focus only on the perturbation of basic frequency, a sketch of the coupling between reshock and RT stabilization effect, as shown in Figure 9, can facilitate to understand why the normal PI does not occur in Case I1. According to the model proposed by Taylor [6] with small perturbations, the classical RT stabilization effect owns an essentially periodic oscillatory behavior, i.e., the initial positive amplitude will reduce to negative and then reversely to positive again, behaving as an infinite loop if viscosity is neglected. In the converging case, however, the period would be shortening with time because the adverse pressure gradient becomes larger and larger.

As demonstrated by experiment and computation, the amplitude may reduce to negative induced by the RT stabilization effect in a light/heavy imploding configuration. Whether the normal PI occurs after reshock is dependent on the reshock-time. For small initial amplitudes, a critical state, i.e., the amplitude reduces to zero, denoted by P_1 in Figure 9 exists before the RTPI occurs. If the reflected shock impinges the evolving interface before the critical state, such as P_0 moment in the first decline stage, the reflected shock will add a negative growth rate ($-v_{\mathrm{RE}}$ which is approximately proportional to the amplitude at the reshock-time) to the negative growth rate caused by the RT stabilization effect ($-v_{\mathrm{RT}}$), resulting in a quickly normal PI. Under this condition, a RTPI will not occur. Coincidentally, if the reflected shock encounters the interface at P_1 moment, the reflected shock will not affect the perturbation growth rate, while the amplitude will continuously reduce to negative because of the RT stabilization effect. At this moment, the perturbation amplitude is zero, but the negative growth rate caused by the RT stabilization effect ($-v_{\mathrm{RT}}$) is the largest. If the reflected shock arrives at the interface after the critical moment, the RTPI will first occur. An additional critical state, as denoted by P_3 where the amplitude is maximal and the growth rate induced by the RT stabilization effect is zero, exists theoretically. If the reflected shock reaches at P_3 moment, the positive growth rate induced by the reflected shock ($+v_{\mathrm{RE}}$) is maximum, and will entirely dominate the interface because v_{RT} is zero. Finally, the reflected shock will result in occurrence of a normal PI. From P_1 to P_3 moments, the growth rate caused by the RT stabilization effect changes from the maximum to zero, while the growth rate caused by the reflected shock varies from zero to the maximum. When the reflected shock collides with the interface at the moment between P_1 and P_3, the reflected shock will add a positive v_{RE} to the negative v_{RT}. There will be a balanced state as indicated by P_2 at which the positive v_{RE} will exactly offset the negative v_{RT}. At the moments between P_1 and P_2, the positive v_{RE} cannot offset the negative v_{RT}, but only decays the negative growth rate. As a result, a normal PI will not occur. At the moments between P_2 and P_3, the positive v_{RE} exceeds the negative v_{RT}, and will lead to the emergence of a normal PI. Further, if the reflected shock reaches at the moments between P_3 and P_4, where P_4 is also a critical state with the maximum positive v_{RT} and zero amplitude, the reflected shock will add a positive v_{RE} to the positive v_{RT}, leading to occurrence of a normal PI quickly. If the periodic oscillation can develop to further stage before reshock, different types of the coupling between periodic RT stabilization effect and reflected shock may occur. In the present work, the state between P_0 and P_1, the critical state P_1, and the state between P_1 and P_2 are found in the Cases I3, I2 and I1, respectively. Features of the interface at different reshock times are summarized in Table 2.

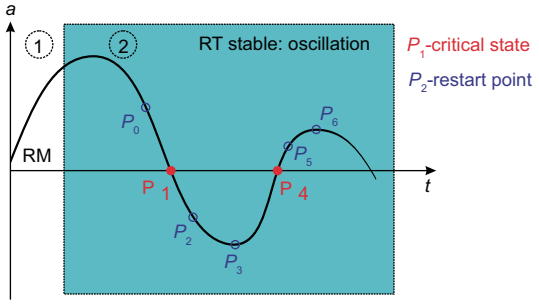

Figure 9 (Color online) RT periodic phase diagram without considering the reshock.

3.2 Effect of azimuthal mode number on critical initial amplitude

The critical state before reshock is a competitive result between the RT stabilization effect and the RM instability. Note that the increase of azimuthal mode number k_0 promotes both

Table 2 Features of the interface at different reshock times

Reshock time	v_{RT}	v_{RE}	State
$< P_0, P_1 >$	–	–	Normal PI
P_1	MAX –	0	First critical
$< P_1, P_2 >$	–	+	RTPI
$< P_2, P_3 >$	–	+	Double PI
$< P_3, P_4 >$	+	+	Double PI
P_4	MAX +	0	Second critical
...	...	...	...

RM instability and RT stabilization effect. The influence of k_0 on the critical state can be assessed by finding the critical a_0 for different k_0. Other parameters of (M_0, A, R_0) = (1.26, 0.68, 195 mm) are unvaried. Here keeping the parameters of (M_0, A, R_0) unchanged is categorized as Case I for the following discussion. The variation of critical a_0 with k_0, termed as critical line, is given in Figure 10. Although the amplitude of the basic mode $a(k_0)$ cannot thoroughly describe the interface morphology when k_0 is large because of the strong nonlinearity, it can also be regarded as a meaningful assessment of the competition between the RM instability and the RT stabilization effect. One can find that a higher k_0 generally needs a smaller a_0 to achieve the critical state. For the same a_0, a higher k_0 strengthens the contribution to the RM instability more than to the RT stabilization effect provided that the time scales of RM instability and RT stabilization effect are the same. Besides, once k_0 is smaller than 14, a RTPI will not occur no matter what a_0 is. Therefore, k_t = 14 is defined as the threshold k_0 for Case I. Further, a special k_0 (named k_s) corresponding to a maximum critical a_0 (a_{0p}) exists. The critical a_0 increases (decreases) with k_0 growing when k_0 is smaller (larger) than k_s. The reason of existing this maximum critical value may lie in the different response of the RM

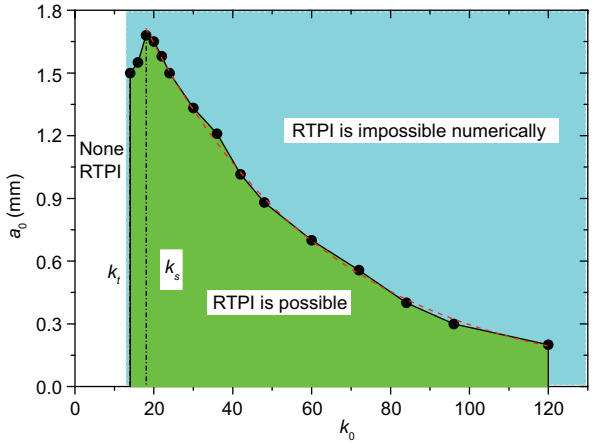

Figure 10 (Color online) The effect of azimuthal mode number k_0 on critical initial amplitude a_0. k_t and k_s are truncation and special azimuthal mode numbers, respectively. The dashed line represents fitting curve from attenuation function, and similarly hereinafter.

instability and the RT stabilization effect for different mode numbers. The RM instability favors the growth of the fundamental mode since it dominates in the linear stage, and the RT stabilization effect reduces higher modes more significantly because it is exerted on an involving interface. Therefore, the maximum critical a_{0p} (k_s) represents the balance of the RM instability and the RT stabilization effect.

More attempts of two Bell models for predicting the amplitude growth are implemented by varying (k_0, a_0). It is surprising that for k_0 = 20, the RTPI will always occur for any a_0, which is not true obviously. Moreover, a k_t is predicted according to the models of Bell, and the RTPI will (will not) occur for any a_0 when $k_0 > k_t$ ($k_0 < k_t$). For finding the k_t, three situations with different startup times are adopted to initiate the calculation: (1) the startup time is ignored and the 0^+ moment is adopted; (2) the startup time of 152 μs for k_0 = 20 is adopted; (3) the variation of startup time with inverse ratio of k_0 is adopted. For varying (k_0, a_0), the k_t for three startup times are calculated to be 12.99, 12.75 and 13.11, respectively, according to the incompressible model, and 12.58, 12.50 and 12.62, respectively, based on the compressible model. As a result, although the Bell models cannot correctly predict the interface development for a long time and the RTPI, they can give a reasonable prediction of k_t. For simplicity, the startup time is ignored in following calculations.

3.3 Parametric study of the critical line

We shall examine the variation of critical a_0 with k_0 by changing other initial parameters (M_0, A, R_0) and discuss the influences of initial parameters on k_t and k_s. As listed in Table 3, only one parameter will change in Cases II-VII compared with Case I. For all cases, the pure N_2 with a density of 1.18 kg/m^3 and the specific heat ratio of 1.4 at initial T_0 = 288 K and p_0 101325 Pa is chosen as the ambient gas.

In Cases II and III, the heavy gas is changed to pure R_{22} and a mixture of SF_6 and N_2 (30%SF_6+70%N_2, volume fraction), respectively. Inevitably, both the specific heat ratio γ_2 and the density of the heavy gas ρ_2 will be changed when us-

Table 3 The physical parameters in each case

Case	Gas 2	γ_2	ρ_2 (kg/m^3)	A	R_0 (mm)	M_0
I	SF_6	1.094	6.177	0.68	195	1.259
II	R_{22}	1.172	3.657	0.512	195	1.259
III	30% SF_6+70% N_2	1.2024	2.682	0.389	195	1.259
IV	SF_6	1.094	6.177	0.68	195	1.156
V	SF_6	1.094	6.177	0.68	195	1.515
VI	SF_6	1.094	6.177	0.68	295	1.259
VII	SF_6	1.094	6.177	0.68	97.5	1.259

ing a different heavy gas. Nevertheless, the Atwood number A is believed to dominate the whole process. The comparison of critical lines among Cases I, II and III is shown in Figure 11. It is obvious that the case with a smaller A owns a larger k_t (k_t = 24 in Case II and 34 in Case III). Besides, for Cases II and III, k_t are estimated to be 22.75 and 35.43, respectively, from Bell's incompressible model, and to be 21.57 and 32.98, respectively, from Bell's compressible model. Again, the theoretical predictions match well with the numerical results. Furthermore, a smaller A corresponds to a smaller a_{0p}, and the critical line reduces more slowly as k_0 increases.

The critical lines of Cases I, IV and V are numerically calculated and compared in Figure 12 to illustrate the effect of initial imploding shock strength M_0. It is found that a stronger imploding shock will lead to a smaller k_t (k_t = 18 in Case IV and 10 in Case V) and a lower a_{0p}. For Cases IV and V, k_t predicted by the two Bell models are 18.12 and 10.13, respectively, based on incompressible assumption, and 17.75 and 9.44, respectively, according to compressible simplification. Similarly, the theoretical predictions coincide well with the numerical results.

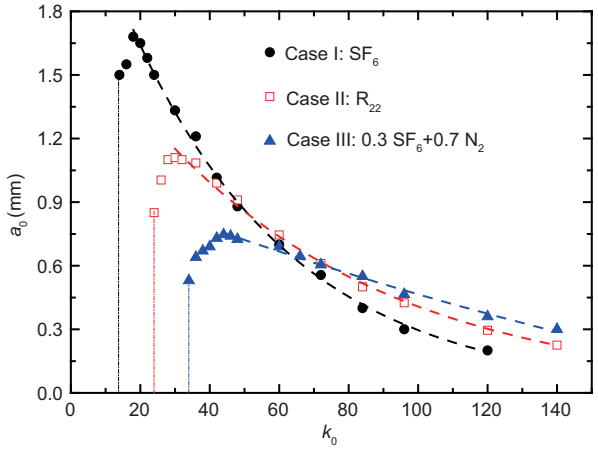

Figure 11 (Color online) Comparison of the critical lines among Cases I, II and III, showing the effect of initial Atwood number.

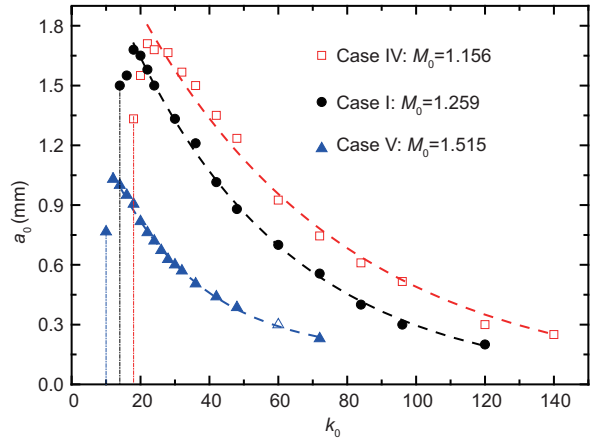

Figure 12 (Color online) Comparison of the critical lines among Case I, IV and V, showing the effect of initial imploding shock intensity.

As shown in Figure 13, the comparison of critical lines among Cases I, VI and VII is given for demonstrating the effect of initial interface radius R_0. Obviously, k_t is independent on the interface radius R_0. The ratios of a_{0p} in Cases VI and VII over a_{0p} in Case I are calculated to be 1.511 and 0.588, approximately corresponding to the ratios of initial interface radius of 1.5 and 0.5, showing an approximately proportional relation of a_{0p} to R_0. Similarly, k_t predicted by the two Bell models are 13.05 and 12.48, respectively, based on incompressible assumption, and 12.61 and 12.11, respectively, based on compressible simplification.

From discussion above, similarities can be found among the critical lines for different conditions, including the existence of a k_t and a maximum critical amplitude a_{0p} at k_s. Besides, the critical amplitude experiences a slow attenuation after k_s. According to the exponential attenuation function, $a_0 = B\exp(-k_0/d) = B_1\exp[(k_s - k_0)/d]$, where $B_1 = B\exp(-k_s/d) \approx a_{0p}$, the variations of critical amplitude with k_0 are obtained, as shown in Figures 11-13 by dashed lines. The parameters of B_1 and d are listed in Table 4, together with other parameters. From the comparison, one can conclude that the reduction rule of critical amplitude with k_0 conforms to an exponential attenuation function.

4 Summary

A series of numerical simulations on the converging Richtmyer-Meshkov (RM) instability are carried out based on an upwind CE/SE method to investigate the Rayleigh-Taylor effect on phase inversion (RTPI), which was firstly observed in our previous experiment. The previous experi-

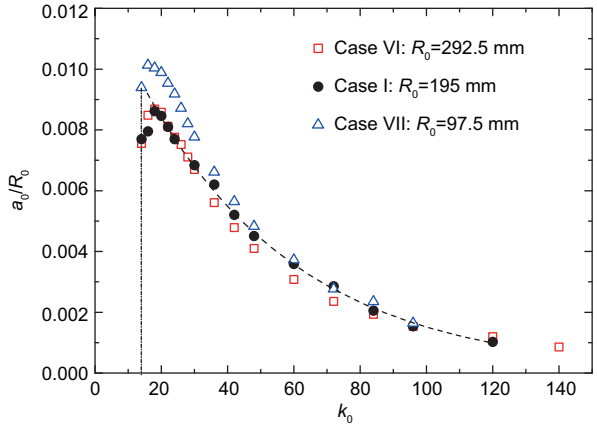

Figure 13 (Color online) Comparison of the critical lines among Case I, VI and VII, showing the effect of initial interface radius.

Table 4 Key values on the critical lines for all cases, and the coefficients of the exponential decay function

Case	k_t	k_s	a_{0p} (mm)	B_1 (mm)	d
I	14	18	1.68	1.712	46.738
II	24	30	1.11	1.152	67.309
III	34	44	0.747	0.767	107.766
IV	18	22	1.71	1.803	59.833
V	10	12	1.03	1.035	35.136
VI	14	18	2.54	2.593	42.015
VII	14	16	0.988	1.042	42.742

ment proved that the 3D effect of interface strongly suppresses the amplitude growth, and facilitates the RTPI occurrence. In this work, a 2D single-mode interface is adopted to eliminate the 3D effect, and the RT stabilization effect on the RTPI can be highlighted.

Firstly, the influence of the initial amplitude on the RTPI is investigated. The evolution of interface with different initial amplitudes indicates that a small initial amplitude favors the RTPI emergence, and, interestingly, a critical state with a zero-amplitude of the interface at the reshock exists for a special initial amplitude. For the critical case, three models are adopted to estimate the amplitude growth, and the models are found to be invalid at late stages possibly because of the flow compressibility. After reshock, a normal phase inversion does not occur for the case in which the RTPI occurs, and a periodic RT phase diagram is adopted to interpret the mechanism. It is concluded that whether a normal phase inversion occurs or not is dependent on the competition between RT stabilization effect and RM instability caused by reflected shock.

Then the variation of critical amplitude with the azimuthal mode number, termed as critical line, is numerically solved. The results show that there is a threshold azimuthal mode number (k_t) below which the RTPI will not occur for any initial amplitude, and there is also a special azimuthal mode number (k_s) at which the critical amplitude is the largest. It is observed that the critical line first increases and subsequently declines separated by k_s, and the reduction rule can be well described by an exponential decay function. Though the (incompressible or compressible) Bell models cannot describe the amplitude growth for a long period, they both provide a reasonable prediction of k_t. Further, a parametric study is performed to evaluate the influences of Atwood number A, shock Mach number M_0 and initial radius of the interface R_0 on the critical line. It is found that the k_t is significantly affected by A and M_0, but is insensitive to R_0. Specifically, a larger A will result in a smaller k_t and a larger peak of the critical amplitude, while a stronger shock contributes to the decline of both k_t and peak of the critical amplitude. Moreover, the peak of the critical amplitude is approximately proportional to R_0. As a result, a larger R_0 not only results in a long-term RT stabilization effect, but also owns a larger critical amplitude. In most previous converging RM instability studies, the initial amplitude is generally large enough compared with the critical amplitude, and, therefore, the RTPI phenomenon cannot be observed.

This work was supported by the National Natural Science Foundation of China (Grant Nos. 11772329, 11802304, and U1530103), the Science Challenge Project (Grant No. TZ2016001). Prof. Wen and Dr. Zhang thank the Research Grants Council, Hong Kong (Grant No. 152151/16E).

1 R. D. Richtmyer, Comm. Pure Appl. Math. **13**, 297 (1960).
2 E. E. Meshkov, Fluid Dyn. **4**, 101 (1972).
3 J. Lindl, O. Landen, J. Edwards, and E. Moses, Phys. Plasmas **21**, 020501 (2014).
4 J. Yang, T. Kubota, and E. E. Zukoski, J. Fluid Mech. **258**, 217 (1994).
5 W. Arnett, J. Bahcall, R. Kirshner, and S. Woosley, Annu. Rev. Astron. Astrophys. **27**, 629 (1989).
6 G. Taylor, Proc. R. Soc. Lond. A **201**, 192 (1950).
7 O. Sadot, L. Erez, U. Alon, D. Oron, L. A. Levin, G. Erez, G. Ben-Dor, and D. Shvarts, Phys. Rev. Lett. **80**, 1654 (1998).
8 N. J. Zabusky, Annu. Rev. Fluid Mech. **31**, 495 (1999).
9 M. Brouillette, Annu. Rev. Fluid Mech. **34**, 445 (2002).
10 B. D. Collins, and J. W. Jacobs, J. Fluid Mech. **464**, 113 (2002).
11 Y. Liang, Z. G. Zhai, and X. S. Luo, Sci. China-Phys. Mech. Astron. **61**, 064711 (2018).
12 Z. Wu, S. Huang, J. Ding, W. Wang, and X. Luo, Sci. China-Phys. Mech. Astron. **61**, 114712 (2018).
13 G. Bell, *Taylor Instability on Cylinders and Spheres in the Small Amplitude Approximation*, Technical Report LA-1321 (Los Alamos National Laboratory, Los Alamos, 1951).
14 M. S. Plesset, J. Appl. Phys. **25**, 96 (1954).
15 K. O. Mikaelian, Phys. Fluids **17**, 094105 (2005).
16 C. Matsuoka, and K. Nishihara, Phys. Rev. E **74**, 066303 (2006).
17 W. Liu, C. Yu, W. Ye, L. Wang, and X. He. Phys. Plasmas **21**, 062119 (2014).
18 L. Wang, J. Wu, H. Guo, W. Ye, J. Liu, W. Zhang, and X. He. Phys. Plasmas **22**, 082702 (2015).
19 L. F. Wang, W. H. Ye, X. T. He, J. F. Wu, Z. F. Fan, C. Xue, H. Y. Guo, W. Y. Miao, Y. T. Yuan, J. Q. Dong, G. Jia, J. Zhang, Y. J. Li, J. Liu, M. Wang, Y. K. Ding, and W. Y. Zhang, Sci. China-Phys. Mech. Astron. **60**, 055201 (2017).
20 J. R. Fincke, N. E. Lanier, S. H. Batha, R. M. Hueckstaedt, G. R. Magelssen, S. D. Rothman, K. W. Parker, and C. J. Horsfield, Laser Part. Beams **23**, 21 (2005).
21 Q. Zhang, and M. J. Graham, Phys. Fluids **10**, 974 (1998).
22 B. Tian, D. Fu, and Y. Ma, Acta Mech. Sin. **22**, 9 (2006).
23 J. G. Zheng, T. S. Lee, and S. H. Winoto, Math. Comput. Simul. **79**, 749 (2008).
24 M. Lombardini, D. I. Pullin, and D. I. Meiron, J. Fluid Mech. **748**, 113 (2014).
25 M. Lombardini, D. I. Pullin, and D. I. Meiron, J. Fluid Mech. **748**, 85 (2014).
26 X. Luo, F. Zhang, J. Ding, T. Si, J. Yang, Z. Zhai, and C. Wen, J. Fluid Mech. **849**, 231 (2018).
27 R. Abgrall, J. Comput. Phys. **125**, 150 (1996).
28 K. M. Shyue, J. Comput. Phys. **142**, 208 (1998).
29 H. Shen, C. Y. Wen, and D. L. Zhang, J. Comput. Phys. **288**, 101 (2015).
30 H. Shen, and C. Y. Wen, J. Comput. Phys. **305**, 775 (2016).
31 S. C. Chang, J. Comput. Phys. **119**, 295 (1995).
32 H. Shen, C. Y. Wen, M. Parsani, and C. W. Shu, J. Comput. Phys. **330**, 668 (2017).
33 Z. Zhai, W. Li, T. Si, X. Luo, J. Yang, and X. Lu, Phys. Fluids **29**, 016102 (2017).
34 H. Shen, and M. Parsani, J. Fluid Mech. **813**, R4 (2017).
35 J. Ding, T. Si, J. Yang, X. Lu, Z. Zhai, and X. Luo, Phys. Rev. Lett. **119**, 014501 (2017).
36 W. Chester, London Edinburgh Dublin Philos. Mag. J. Sci. **45**, 1293 (1954).
37 R. F. Chisnell, J. Fluid Mech. **2**, 286 (1957).
38 G. B. Whitham, J. Fluid Mech. **4**, 337 (1958).
39 M. Lombardini, and D. I. Pullin, Phys. Fluids **21**, 044104 (2009).